Cell Systems, Volume *3*

Supplemental Information

Asymmetric Damage Segregation Constitutes an Emergent Population-Level Stress Response

Søren Vedel, Harry Nunns, Andrej Košmrlj, Szabolcs Semsey, and Ala Trusina

I. CELL CULTURE AND TIME-LAPSE MICROSCOPY

Cells were inoculated from the LB agarose plate in M63 minimal media with selection markers and were grown overnight at the specified temperature in 10 mL tubes in a shaking incubator. Cells were diluted into fresh media (with selection markers etc.) in the morning and left for $\sim$ 2.5 h in the incubator to reach the exponential phase. Experiments were commenced following another dilution.

Low-density cells were transferred to a 1.5% agarose pad (containing all relevant selection markers, antibiotics etc. in same concentrations as in the liquid culture), which was inverted and placed directly on a microscope cover slip (No. 1.5) and sealed with an air-tight top made from a glass cover and PDMS gasket to form a transparent container with cells growing between the cover slip and the agarose. All the components were kept at the target temperature at all times. All experiments were conducted on a Nikon Eclipse Ti microscope fitted with a feedback-controlled heat cage (OkoLab H201 bold line cage incubator), Sutter Instruments Lambda SC shutter and Andor NEO SCC-1758 camera using a Nikon Plan Apo 100X (DIC N2) oil objective, and images acquired using the manufacturer-supplied NIS software.

For each experiment we identified 8-14 isolated single cells on the agar pad, each giving rise to a single colony. Each colony was imaged every 3-4 min in bright field (3.5 V lamp, $\sim$ 60 ms exposure) and every 15 min in YFP fluorescence channel (500 ms exposure). Previous studies have used fluorescence for single-cell segmentation and tracking [1–4]. However, exciting fluorescent markers in cells is known to stress them, so we opted for the less stressing brightfield microscopy. Image segmentation and cell-tracking are performed on brightfield images taken slightly out of focus ($\sim$ half cell diameter) at every time step. We ensured that the resulting cell boundaries are in agreement with in-focus images; fluorescence images are taken in focus.

Mutant: Heat shock stress

Strain and plasmids	Environmental stress	# of independent exp.	# of colonies	# of accepted cells
* MC4100Δ*clpB* w/ClpB-YFP and lacI^q	37 °C	2	10	1756
MC4100Δ*clpB* w/ClpB-YFP and lacI^q	42 °C	2	11	1704

Mutant: Antibiotic stress

Strain and plasmids	Environmental stress	# of independent exp.	# of colonies	# of accepted cells
* MC4100Δ*clpB* w/ClpB-YFP and lacI^q	37 °C + 0.0 µg/mL Km	2	10	1756
MC4100Δ*clpB* w/ClpB-YFP and lacI^q	37 °C + 0.5 µg/mL Km	2	11	1804

Wild-type: Heat shock stress

Strain and plasmids	Environmental stress	# of independent exp.	# of colonies	# of accepted cells
** MC4100 w/lacI^q	37 °C	2	10	2090
MC4100 w/lacI^q	42 °C	2	13	2084

Wild-type: Antibiotic stress

Strain and plasmids	Environmental stress	# of independent exp.	# of colonies	# of accepted cells
** MC4100 w/lacI^q	37 °C + 0.0 µg/mL Km	2	10	2090
MC4100 w/lacI^q	37 °C + 0.5 µg/mL Km	3	16	1948

*This is the same data used for reference in both mutant studies.
**This is the same data used for reference in both wild-type studies.

TABLE S1. Summary of all Experiments Reported in this Study, Related to Experimental Procedures. We simultaneously tracked 8-14 independent and non-interacting colonies in each experiment as described in Supplemental Experimental Procedures, Sec. I.

II. CHEMICALS AND REAGENTS

All reagents were purchased from Sigma-Aldrich except for agarose and IPTG, which was purchased from Serva (Agarose SERVA). Reagents were dissolved in either ethanol (chloramphenicol) or DI water (all other reagents) and filter-sterilized prior to use.

III. STATISTICAL ANALYSIS

III.1. Statistical significance of different doubling times between lineage-groups

Supplementary to Figures 2C and 3A,B and Figures S3C,G,H,M. Since not all lineage-groups exhibit normally distributed doubling times, we used non-parametric statistics, and to furthermore avoid artifacts of low sample sizes, we used both the two-sample Kolmogorov–Smirnov test and the Wilcoxon rank-sum/Mann–Whitney U-test with 5% significance level. As shown by black outline in main Figure 3A,B and Figures S3C,G,H,M, we do observe significant difference for groups which are separated further in the population tree. For groups with little separation, the within-group noise is comparable with the between-group variation. We note that significantly increasing the number of cells in our experiments will lead to statistically significant differences between a larger set of groups, as is illustrated by the extensive data set by Stewart *et al.* [1] (see Figure S2).

III.2. Generating null-distributions for populations of lineage-grouped doubling times

Supplementary to Figures 2D, and 3C,D and S3D,E,I,K N,O. We generated the non-ADS null distributions for the lineage-grouped data sets as follows. Using the unfiltered (including within-group variations) lineage-sorted data, we randomly shuffled two cells between groups and repeated this process 100 times the total number of cells in all groups to get good mixing while preserving the number of cells in each group. After shuffling the median of each group was computed and stored, and the process repeated over 500 times, each time starting from the original, unfiltered lineage-sorted data set. The 500 distributions of medians from each reshuffling process were pooled to generate the presented null distribution. The point of repeating 500 times is to get an idea of how much the data shifts around as a consequence of a reshuffling event, which relates to the variance of the null distribution.

III.3. Investigation of statistically significant difference of population diversities σ

Supplementary to Figures S3A,F,L,P. To test if the population diversities (equivalent to widths of distributions of doubling times), σ, are significantly different at low and high stress we use bootstrapping to estimate the statistical significance of the difference

$$\Delta\sigma = \sigma_{42\ ^\circ\mathrm{C}} - \sigma_{37\ ^\circ\mathrm{C}} \tag{S1}$$

of the population diversities $\sigma_{42\ ^\circ\mathrm{C}}, \sigma_{37\ ^\circ\mathrm{C}}$ at 42 °C and 37 °C respectively. To account for the fact that the associated null distributions change between the two temperatures, see Figure 3C in the main text. we performed the following statistical analysis

- Step (i) perform bootstrapping (random sampling with replacement) on lineage grouped data at 37 °C (using the same number of data points as the original data set) to obtain a value for $\sigma_{37\ ^\circ\mathrm{C}}$.
- Step (ii) perform the same analysis on the lineage-grouped data at 42 °C to obtain a value for $\sigma_{42\ ^\circ\mathrm{C}}$.
- Step (iii) compute $\Delta\sigma$ from Eq. (S1).
- Step (vi) repeat steps $(i) - (iii)$ 10^4 times to obtain distribution of differences $\Delta\sigma_{\mathrm{LS}}$.
- Step (v) repeat steps $(i) - (iv)$ using the associated null-distribution data instead of the lineage-grouped data at each temperature to obtain distribution of differences $\Delta\sigma_{\mathrm{null}}$.

The null-distribution difference $\Delta\sigma_{\mathrm{null}}$ reflects the variation in sample-size in lineage groups between the two temperatures. The population diversities at low and high stress are statistically significantly different, if the distribution of actual differences $\Delta\sigma_{\mathrm{LS}}$ is significantly different from the distribution of differences in corresponding null distributions$\Delta\sigma_{\mathrm{null}}$. This is indeed the case as shown in Figure S3A,F,L,P. The distributions under all stresses are significantly different ($P<0.01$, two-sample t-test analysis). Thus the population diversity σ increase significantly under heat and kanamycin stress in both wild-type (MC4100) and MC4100ΔClpB+ ClpB-YFP strains.

III.4. Aggregate data statistics

Supplementary to Figures 4 and S4. At any pole age, the aggregate data follows a binomial distribution with an age-specific probability p_a of having an aggregate. For the case with N^a_{agg} aggregates and N^a_{cells} cells we compute

the frequency (estimated probability) of aggregates $f_a = \frac{N^a_{\text{agg}}}{N^a_{\text{cells}}}$, and the standard deviation of the frequency $\sigma_{f_a} = \sqrt{\frac{f_a(1-f_a)}{N_{\text{cells}}}}$ using the standard formulae for the binomial distribution.

III.5. Standard error of the mean for populations of cells

Supplementary to Figures 5A and S5D. Distributions of single-cell doubling times were not normal, so we used bootstrapping to obtain standard error of the mean (SEM): we resampled the data with replacement to obtain a single realization of the population mean, and repeat a total of 10^4 times, thereby producing a distribution of means. This resulting distribution of means follows a normal distribution and is thus well-characterized by its standard deviation, which is the SEM.

III.6. Difference of doubling times ΔT of damage accumulating/evading lineages

Supplementary to Figure 5A, S5A and S5D. In Figures 5A and S5D we show the difference in doubling times between the consecutively damage-accumulating and consecutively damage-evading lineages (corresponding to all-green and all-magenta lineages in Figure 2A) originating from the same ancestor. We always start from an ancestor which has once undergone damage-evading event and at each generation record doubling times of consecutively damage-accumulating cells. This produces a sequence of doubling times $T_{\text{accum}}(n)$ as a function of generation number n following the initial cell for damage-accumulating. Repeating the analysis for the consecutively damage-evading lineage produces the sequence T_{evad}. The difference ΔT is at each generation n the difference between the two sequences, $\Delta T(n) = T_{\text{accum}}(n) - T_{\text{evad}}(n)$.

The repeats in the experimental data are averaged at each generation n before subtracting; we use the $\overline{\ }$ to denote average within each generation of such a lineage, our experimental results are expressed as $\Delta\overline{T}(n) = \overline{T}_{\text{accum}}(n) - \overline{T}_{\text{evad}}(n)$.

III.6.1. Analytical expression

Experimentally, cells were grown at some temperature for ~ 24 h prior to the start of an experiment, and they have therefore adapted to this state. Since the state of the initial cell in an experiment is unknown, we take it to be the average $\langle D\rangle$. Since $\langle D\rangle$ scales linearly with λ we will also write $\lambda\langle\tilde{D}\rangle = \langle D\rangle$. Damage-accumulating lineages inherit the fraction $(1+a)/2$ of ancestor damage, while damage-evading inherit $(1-a)/2$ of ancestor damage.

Starting from the average damage $\langle D\rangle$, the damage in the damage-accumulating sibling in the first few generations is

$$\begin{aligned}
&\text{Gen. 0}: \quad \lambda\langle\tilde{D}\rangle,\\
&\text{Gen. 1}: \quad \lambda\left[1+\frac{1+a}{2}\langle\tilde{D}\rangle\right],\\
&\text{Gen. 2}: \quad \lambda\left[1+\frac{1+a}{2}\left[1+\frac{1+a}{2}\langle\tilde{D}\rangle\right]\right] = \lambda\left[1+\frac{1+a}{2}+\left(\frac{1+a}{2}\right)^2\langle\tilde{D}\rangle\right],
\end{aligned} \tag{S2}$$

Thus, the damage in the consecutive old-pole lineage at generation q after the common ancestor is given by

$$H_{\text{old}}(q) = \lambda\left[\sum_{i=0}^{q-1}\left(\frac{1+a}{2}\right)^i + \left(\frac{1+a}{2}\right)^q\langle\tilde{D}\rangle\right] \text{ for } q>0,$$

Similarly, we find for the new-pole history starting from average damage $\langle D\rangle$

$$H_{\text{new}}(q) = \lambda\left[\sum_{i=0}^{q-1}\left(\frac{1-a}{2}\right)^i + \left(\frac{1-a}{2}\right)^q\langle\tilde{D}\rangle\right] \text{ for } q>0.$$

The difference $\Delta T(q)$ of doubling time histories (old pole minus new pole) at generation q following the common ancestor is therefore given by

$$\begin{aligned}\Delta T(q) &= t_{\min} + \mu H_{\text{old}}(q) - [t_{\min} + \mu H_{\text{new}}(q)] \\ &= \mu\lambda\left(\left[\sum_{i=0}^{q-1}\left(\frac{1+a}{2}\right)^i + \left(\frac{1+a}{2}\right)^q \langle\tilde{D}\rangle\right] - \left[\sum_{i=0}^{q-1}\left(\frac{1-a}{2}\right)^i + \left(\frac{1-a}{2}\right)^q \langle\tilde{D}\rangle\right]\right),\end{aligned} \tag{S3}$$

which holds for $q > 0$.

This formula (Eq. (S3)) was fitted to the experimental data in Figure 5A and S5D.

III.6.2. Linear scaling of $\Delta T(n)$ under different stresses

Equation S3 predicts that the difference $\Delta T(n)$ will follow almost the same functional form under different stresses, since the stress-dependence of $\langle D\rangle$ is secondary compared to the linear dependence of the prefactor. Higher stresses (larger λ) shift the the curve up, so plotting against each other $\Delta T(n)$ under two different stresses 1 and 2, the slope α of the curve will be well approximated by the ratio of their stress levels $\alpha = \lambda_2/\lambda_1$. This prediction is confirmed from our experimental data in Figure S5A.

III.7. Fitting population model to experimental data for the doubling-time difference of damage-accumulating/evading lineages $\Delta\overline{T} = \overline{T}_{\text{accum}} - \overline{T}_{\text{evad}}$

We fit our population model using both constant asymmetry and damage-dependent asymmetry to the experimental population data for the difference of doubling times of the damage-accumulating/evading lineages. For the analytical model we use Eq. (S3), while we rely on simulations for the model with damage-dependent asymmetry.

We fit simultaneously to the data under low and high stress, because both can be used to infer system-specific parameter values, while each independently can be used to infer the specific stress-level. These fits serve the dual purpose of (*i*) determining which of the two models best describe the data (i.e. as a test of whether damage-dependent asymmetry indeed is detectable at the population level), and (*ii*) determine the remaining free model parameters μ, and λ under both low and high stress, henceforth denoted λ_{L} and λ_{H}. The minimum doubling time $t_{\min}$ is not know directly from our measurements, and the difference of doubling times $\Delta T(n)$ depends only very weakly on the exact value (tested the plausible range $t_{\min} \in [15; 30]$ min). We set $t_{\min} = 22$ min (corresponding to the low stress conditions in our data) in all fitting procedures.

We have fitted the experimental data using the analytical model with the value $a = c_1 = 0.7411$ obtained above from the aggregate inheritance data (see Table S2), the theoretical optimum at $a = 1$, and using damage-dependent asymmetry with parameters from Table S2. We find that model with damage-dependent asymmetry is by far superior, indicating that experiments support only $a(D)$ (Akaike weight $w \approx 0.99$) and exclude models with constant asymmetry.

III.8. Analyses of the damage-dependent asymmetry

Using the experimental data on aggregate area asymmetry at cell division (Figure S5B), we can estimate the asymmetry function $a = a(D)$ that this data implies, see Figure S5C. The asymmetry is clearly not constant, but has sigmoidal dependence on aggregate area. Sigmoidal functions assures that asymmetry will lie between physiologically plausible values 0 and 1. We find that the best fitting function is $a = \frac{c_1 + D^{c_3}}{c_2 + D^{c_3}}$, with parameters shown in Figure S5C. The parameter values obtained from least-squares fitting.

III.9. Calculation of AIC_{c} values in the Akaike Information Criterion

Formally, the value of AIC_{c} is given by

$$\text{AIC}_{\text{c}} = -2\log\left(\mathcal{L}(\hat{\theta}|y)\right) + 2K + \frac{2K(K+1)}{n-K-1}, \tag{S4}$$

where $\hat{\theta}$ is a vector containing the model parameters (the model-specific c_i's and the unknown "noise" variance σ of the residuals) maximizing the likelihood function given the experimental data y, $\mathcal{L}$ is the maximized likelihood

Condition	Model	λ_L [μm^2] (37C, no KM)	λ_H [μm^2]	μ [min μm^{-2}]	χ^2_{red}	Akaike weight, w
MC4100ΔclpB	Const. asym. $a = 0.7411$	0.1330	0.4797	3.9723	12.7834	1.098×10^{-3}
Heat stress	Const. asym. $a = 1$	0.1042	0.3779	3.1468	12.2756	9.3149×10^{-3}
	Dam. dep. asym.	**0.0869**	**0.1610**	**12.8364**	**4.0668**	**0.9896**
MC4100ΔclpB	Const. asym. $a = 0.7411$		0.3001		9.0944	2.3674×10^{-4}
Kanamycin stress	Const. asym. $a = 1$	same as above	0.2294	same as above	6.9103	4.3942×10^{-3}
	Dam. dep. asym.		**0.1228**		**3.3245**	**0.9954**
MC4100	Const. asym. $a = 0.7411$	0.1995	0.3343	3.5126	5.1804	8.955×10^{-5}
Kanamycin stress	Const. asym. $a = 1$	0.1484	0.2648	2.7448	3.8387	1.9786×10^{-3}
	Dam. dep. asym.	**0.1188**	**0.1693**	**6.9518**	**1.2389**	**0.9979**
MC4100	Const. asym. $a = 0.7411$		0.2418		4.2229	1.457×10^{-4}
Heat stress	Const. asym. $a = 1$	same as above	0.1905	same as above	3.0803	3.290×10^{-3}
	Dam. dep. asym.		**0.1417**		**1.0000**	**0.9966**

TABLE S2. Supporting table for Figure 5A and Figure S5 showing best-fit parameters λ_L, λ_H and μ for the three models: "Const. asym. $a = 0.7411$", "Const. asym. $a = 1$" and "Dam. dep. asym." with $t_{min} = 22$ min. The low-stress parameter, λ_L, corresponds to the condition of 37C and no Kanamycin, thus we use same values of λ_L for the same strain. Stress parameter is expressed in units of aggregate size. Last two columns show the goodness of the fit: the reduced χ^2-values (χ^2_{red}) for each model indicating how well it fits the experimental data relative to the uncertainty of the experimental measurement and the Akaike weights w which estimates the relative level of support in favor of each model best describing the data relative to the two other models. The best model (highlighted in boldface) is damage-dependent asymmetry according to the Akaike weights, while the two other models are doing substantially worse. The residuals of this best model is on par with the measurement error and are consequently as good as can be expected.

function (likelihood function evaluated at its maximum point, i.e. at the parameter values $\hat{\theta}$) of the model given the experimental data y, n is the sample size and K is the number of free parameters in the model together with the unknown noise variance of the residuals (that is, $K = \tilde{K} + 1$ where $\tilde{K}$ is the number of free parameters in the model, e.g. the number of c_is). The last term on the right hand side of this equation is the second-order correction term needed to provide better estimates at small sample sizes.

We used least-squares fitting to obtain the optimal parameters. For our models, the least-squares optimal parameters are related to the maximum-likelihood optimal parameters through a simple relationship, assuming the residuals follow a normal distribution [5]. This relationship stipulates

$$\log\Big(\mathcal{L}(\hat{\theta}|y)\Big) \approx -\frac{n}{2}\log\hat{\sigma}^2 \tag{S5}$$

where $\hat{\sigma}^2 = \sum_i \epsilon_i^2/n$ is given in terms of the squared residuals ϵ_i from the least-squares fit and the number of samples n. The approximation in Eq. (S5) consists of dropping constant terms which are the same for all models, which become irrelevant since only the differences in AIC_c values between models is of importance. We therefore replace Eq. (S4) by

$$AIC_c = n\log\left(\hat{\sigma}^2\right) + 2K + \frac{2K(K+1)}{n-K-1}, \tag{S6}$$

and use this to compute the AIC_c values. We have checked that using actual maximum likelihood estimation provides numerically indentical results for the c_i's, Δ and w for all three models, with irrelevant differences in raw AIC_c values between the two approaches a consequence of the approximation in Eq. (S5).

III.10. Quantification of the ADS-unrelated cell-to-cell variation

The statistical similarity of the within-age-group noise at each temperature allowed us to pool all noise from each age group. Interestingly, the resulting distributions, given as full lines in Figure S5, appear fairly similar. However, the fold-increase in noise distribution width σ^n is 1.37 between the two temperatures ($\sigma^n_{37\,^\circ C} = 4.97$ min and $\sigma^n_{42\,^\circ C} = 6.79$ min). For comparison the fold-increase in the width σ^{LS} of the distribution of lineage-sorted data is 1.93 ($\sigma^{LS}_{37\,^\circ C} = 1.06$ min and $\sigma^{LS}_{42\,^\circ C} = 2.05$ min). To take into account the difference in means, we computed the coefficient-of-variance of population doubling times $\tilde{C} = \sigma/\langle T\rangle$ for lineage-sorted data and noise (in both cases normalizing the population-mean) at the two stress levels, and found that while the parameter does increase for

the noise distributions by a factor 1.28 (from $\tilde{C} = 0.18$ to $\tilde{C} = 0.23$) this increase is larger for the lineage-sorted data (increase by a factor 1.8; from $\tilde{C} = 0.04$ to $\tilde{C} = 0.07$). These results are conistenet across all the strains and conditions. It follows that the variations of width of whole-population-distributions of doubling times in response to increasing stress are caused primarily by asymmetric damage segregation, and are only secondarily a consequence of noise increasing in response to stress as well.

IV. AGENT-BASED NUMERICAL SIMULATIONS

The models have been implemented in MATLAB R2012b. In all reported cases we have started the simulations from a single cell with 0 inherited damage. MATLAB code for both models will be made available per request.

To simulate the growing population, we first construct the entire population tree for a specified number of generations. Next for each cell in the tree we compute and record cell's damage and doubling time as given in Eq. 1 and 2 in the main text. To extract population quantities such as population-average doubling time, population-distribution of damage etc., we make a second sweep through the population tree and query for any property of interest. Up to ~ 30 generations of cell divisions can be simulated on a laptop within reasonable time (yielding about 10^9 cells).

Since the cells divide a deterministic time $t_{\min} + \mu D$ following last division, and the simulations start from a single cell, there is a transient period when cells are synchronously divide at the same time. After about 10 generations the divisions are slowly desynchronized. The synchronous divisions affect the sampling of distributions of doubling times (one has to go beyond 30 generations to reach steady state distributions) and to avoid it we add small-amplitude zero-mean noise to $t_{\min}$ for 5 consecutive generations to all cells present, starting at generation 5. The amplitude of this noise is $\mu\lambda/5$ but seems to be largely irrelevant within reasonable ranges. By this process we can thus reach a faster convergence of the damage distribution without affecting the population growth rate. This approach is valid as real doubling times are also noisy (see Figure S5E).

IV.1. Simulations with physiological levels of noise, Figure 6A

For these simulationsthe noise is added on the ADS-unrelated minimum generation time $t_{\min}$, by adding a random number ξ to $t_{\min}$ for each cell, with ξ taken from the experimentally determined zero-mean distribution of physiological noise 42 °C shown Figure S5E.

IV.2. Mean and standard deviation of population-distribution of doubling times, Figure 1A-C and 6A

At each time point in the simulations we obtain the instantaneous means of damage $\overline{D}(t)$ and doubling time $\overline{T}(t)$ and width $\sqrt{\overline{T^2} - \overline{T}^2}$ of the population-distribution of doubling time. We store all values starting at $t = 20 \times (t_{\min} + \mu\lambda)$, and for each statistic $\overline{D}(t)$, $\overline{T}(t)$ or $\sqrt{\overline{T^2} - \overline{T}^2}$ obtain a mean and a standard deviation over the storage interval which we use for the true population-averaged values of these statistics $\langle D \rangle$, $\langle T \rangle$ and σ. For each statistic we also estimate and show the variations (standard deviation) across the sampling interval. Results using this approach are given in Figure 1B,C,E.

V. THEORETICAL MODEL

Here we sketche out an overall description of our analytical approach and present the final formulae. The details of model derivation will be published elsewhere.

The whole-population effects of ADS can be analyzed analytically by mapping the problem of ADS to the Ising model in physics[6]. This enables us to relate microscopic details of interactions between ancestral and current cells to the macroscopic observables on the population level, e.g. growth rate and damage distribution among cells. The Ising model describes the behavior of a system of interacting physical particles. Each system state is a specific combination of individual particle states. The particle states are binary (denoted by ± 1 and often referred to as spin up and spin down states), and the probability that a particle occupies a given state is affected by the states of the nearest-neighbor particles. In the one-dimensional case, this corresponds to a linear chain of particles, known as an Ising chain.

Here, we map each lineage in a growing bacterial population onto a unique system state of an Ising chain. A lineage encompasses all known ancestors of a given cell, and every lineage begins with the first cell in the bacterial colony.

Two examples of lineages are highlighted by the green and magenta lines in Figure 1A. The state (± 1) of a single cell within a lineage dictates the amount of damage inherited from its ancestor, preserving the concept of nearest-neighbor interactions. By relating damage inheritance to the division time of a cell (Eq. 2), we find that the sequence of cell states (± 1) within a lineage determines the total time elapsed from the first cell to the most recent division in the lineage. Thus, the time spanned by a lineage is analogous to the energy of a specific Ising chain configuration. The goal is to determine the statistical properties of a bacterial population at time t, which is equivalent to the statistical properties across many Ising chains with fixed system energy E. Thus, by this analogy, statistical moments such as the mean and standard deviation (population width) of e.g. doubling times across the biological population of cells can be computed using the ensemble averages of the equivalent model in statistical physics. This method allows us to derive approximate analytical expressions for the mean doubling time $\langle T\rangle$ and the width σ of the distribution of doubling times.

V.1. Mean and variance of population damage and doubling time

Using these approach we find the following approximate result for the mean doubling time

$$\langle T\rangle \approx t_{\min} + \mu\lambda\left[2 + a^2\lambda\mu\beta\varepsilon^* \frac{(27\beta\varepsilon^*\lambda\mu - 2)a^2 - 18}{8}\right] \quad . \tag{S7}$$

We furthermore find for the width of the population-distribution of doubling times

$$\sigma \approx \frac{\mu\lambda a}{4}\sqrt{20 + a^2\left[4 + \beta\varepsilon^*\lambda\mu\left(-44 - 45\beta\varepsilon^*\lambda\mu + a^2\left\{2 + 9\beta\varepsilon^*\lambda\mu\left[1 + \beta\varepsilon^*\lambda\mu\left(27 + a^2\left\{2 - 18\beta\varepsilon^*\lambda\mu\right\}\right)\right]\right\}\right)\right]} \tag{S8}$$

where $\beta\varepsilon^* = \frac{8\lambda\mu + 4t_{\min} - 2f(a,\lambda,\mu,t_{\min})}{a^2(9+2a^2)\lambda^2\mu^2}$ and $f(a,\lambda,\mu,t_{\min}) = \sqrt{2}\sqrt{8\lambda\mu t_{\min} + 2t_{\min}^2 - \lambda^2\mu^2\left[9a^2\ln 2 - 8 + a^4\ln 4\right]}$. In these expressions, a is the asymmetry parameter, $t_{\min}$ is the minimum damage-independent single-cell doubling time, λ is the amount of acquired environmental damage per generation, and μ is the conversion factor between damage and doubling time. All expressions have been derived assuming $a > 0$.

The two results from Eqs. (S7) and (S8) are given in Figure 1B and E in the main text. We find good agreement with simulation results throughout, except for the width σ for a close to 1 when $\lambda\mu$ is large ($\lambda\mu > 1$), where Eq. (S8) slightly overshoots.

V.2. Special case of symmetric division, $a = 0$

The special case of symmetric division ($a = 0$) is not handled by our approximate analytical expressions, however, in this special case all cells carrying the same amount of damage and divide and average population-properties are identical to single-cell properties; thus, we can easily provide exact analytical expressions for the population behavior.

Inheriting exactly 50 % of the ancestor's damage, the damage in generation n of a single cell starting from 0 damage at the first generation and acquiring λ damage from the environment in each generation, is given by $D(n) = \lambda\sum_{j=1}^{n}\frac{1}{2^{j-1}}$. For large n, this damage stabilizes to a constant level $D(n) = 2\lambda$ because the geometric series $\sum_{j=1}^{n} 1/2^{j-1}$ converges to 2 for $n \to \infty$. In this long-time limit, all cells in the population have the same amount of damage, and so it follows directly that $\langle D\rangle = 2\lambda$ and $\sigma_D = \sqrt{\langle D(n)^2\rangle - \langle D(n)\rangle^2} = 0$. From the relationship between damage and doubling time Eq. (2) in the main text, we find for the distribution of doubling times

$$\langle T\rangle = t_{\min} + \mu\langle D\rangle = t_{\min} + 2\mu\lambda \quad \text{and} \quad \sigma = \mu\sigma_D = 0. \tag{S9}$$

[1] E. J. Stewart, R. Madden, G. Paul, and F. Taddei, PLoS Biology **3**, e45 (2005).
[2] A. B. Lindner, R. Madden, A. Demarez, E. J. Stewart, and F. Taddei, Proc. Nat. Acad. Sci. USA **105**, 3076 (2008).
[3] P. Wang, L. Robert, J. Pelletier, W. L. Dang, F. Taddei, A. Wright, and S. Jun, Curr. Biol. **20**, 1099 (2010).
[4] J. Winkler, A. Seybert, L. König, S. Pruggnaller, U. Haselmann, V. Sourjik, M. Weiss, A. S. Frangakis, A. Mogk, and B. Bukau, EMBO Journal **29**, 910 (2010).
[5] K. P. Burnham and D. R. Anderson, *Model selection and multimodel inference: a practical information-theoretic approach*, 2nd ed. (Springer, 2002).
[6] R. J. Baxter, *Exactly solved models in statistical physics* (Academic Press, 1982).

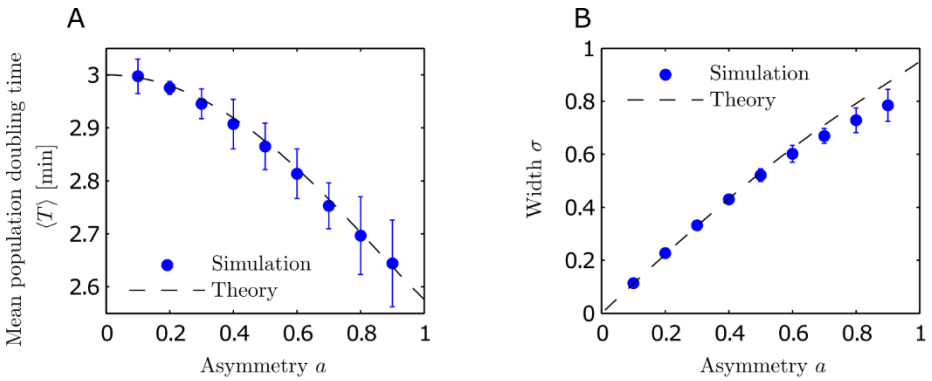

Figure S1. Effects of Asymmetry a on Model Predictions, Related to Figure 1. Errorbars on simulation results indicate standard deviations on the presented metrics. These arise as a consequence of using a stochastic simulation algorithm. **A.** Mean doubling time $\langle T \rangle$ decreases with asymmetry a. Theoretical results computed from Eq. S30. **B.** Width of population-distribution of doubling times σ increases with a, with theoretical prediction given in Eq. S8. Results shown are for the model where all cells have the same asymmetry parameter, t_{min} = 1 min, $\lambda = 1\mu^2$ and $\mu = 1$ min μ^{-2}. Details of theoretical calculations and agent-based simulations are given in Supplemental Experimental Procedures, Sections IV and V.

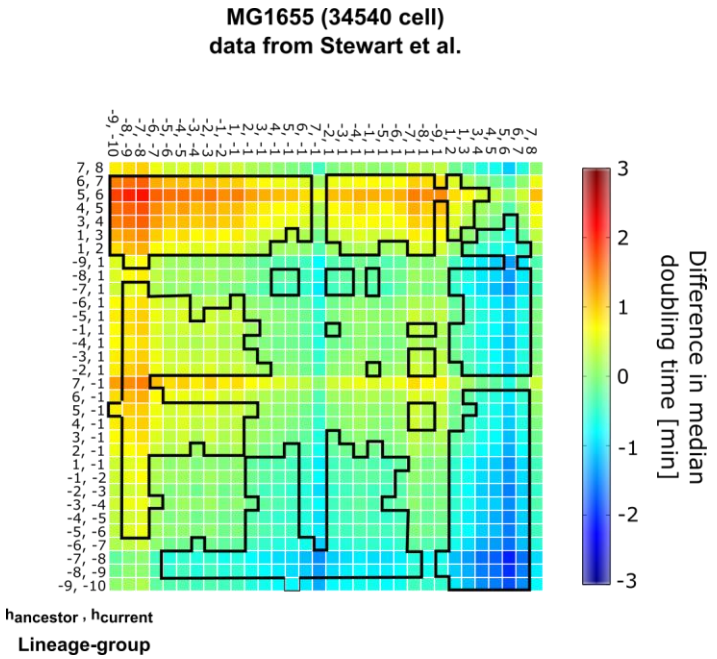

Figure S2. Validation of Lineage-Based Analyses Using Data from Stewart et al.[1], related to Figure 2 **A.** Heatmap of the pairwise differences in median doubling times for each pair of lineage-groups, with notations as in main Figure 2C. Each colored square in the heat map color-codes the difference between the corresponding vertical and horizontal lineage-groups. Significant differences are outlined in black. Statistical significance was computed using the non-parametric Wilcoxon rank-sum test (Mann-Whitney U-test) at the 5% significance level. Similar results are obtained with non-parametric two-sample Kolmogorov-Smirnov test.

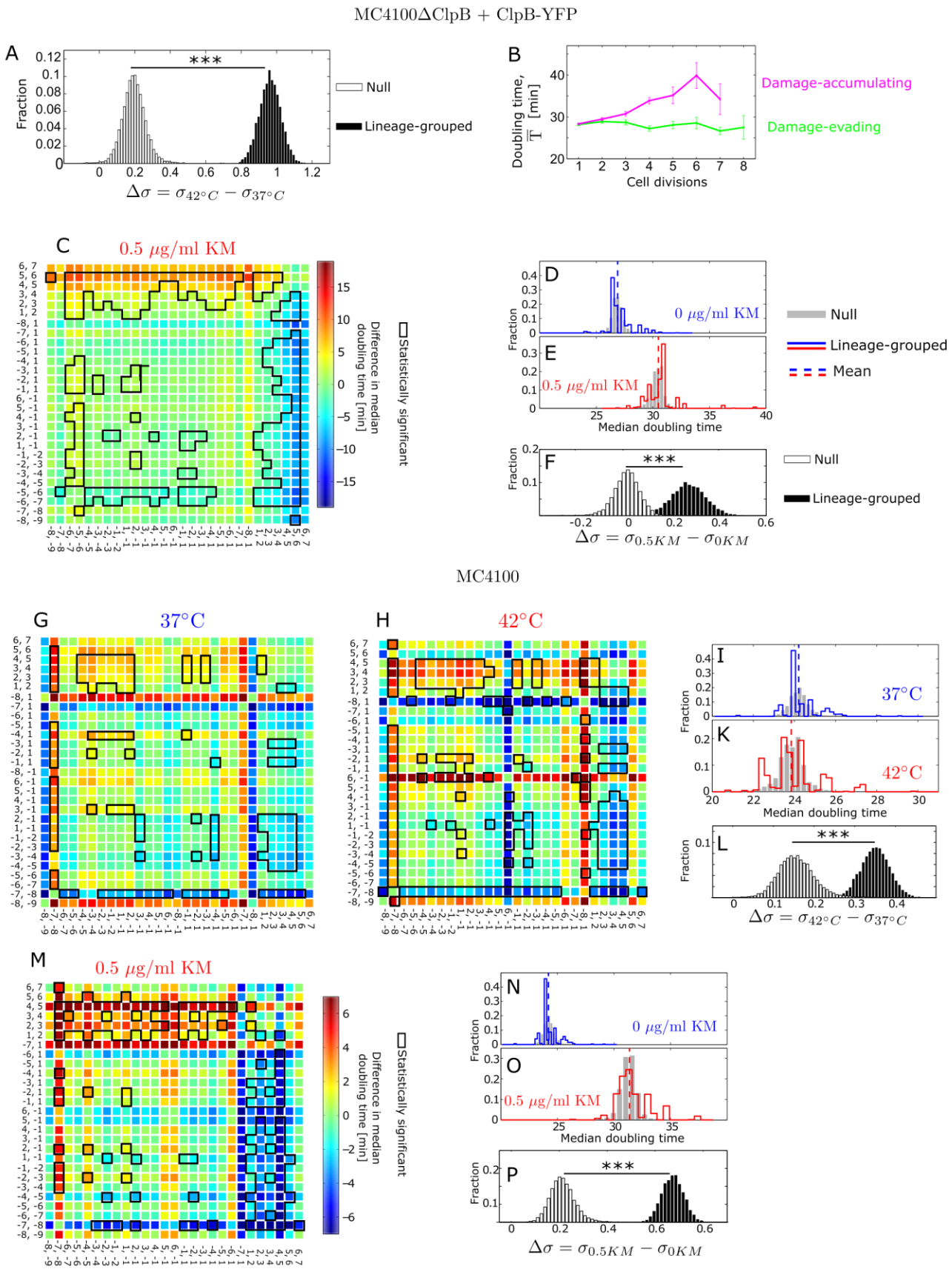

Figure S3. ADS Quantification across Strains and Stresses, Related to Figure 3.
A. The distributions of the differences $\Delta\sigma$ used to statistically test the increase in population

diversity, σ, under heat stress (for data presented in Figure~3C,D). The distributions are obtained as described in Supplemental Experimental Procedures, Sec.III.3. The differences are calculated independently for the lineage-grouped data (filled bars) and the associated null-distribution data (open bars). The population diversity at 42℃, $\sigma_{42^{\circ}\mathrm{C}}$, is statistically significantly different from the population diversity at 37℃, $\sigma_{42^{\circ}\mathrm{C}}$. *** denotes statistically significant difference (P<0.01, by two-sample *t*-test analysis). **B.** Doubling times of lineage-groups with successive rounds of damage-accumulation (or damage-evasion) converge to steady values. We plot the experimentally obtained doubling times of the consecutive old-pole lineage (magenta) and new-pole lineage (green) as a function of the number of generations from the initial cell. Errorbars mark standard error of the mean obtained via bootstrapping.

C. Heatmap, obtained as in Figure 2C, for population of MC4100ΔclpB + ClpB-YFP cells stressed by 0.5 μg/ml kanamycin. The heatmap for unstressed cells is shown in main Figure 3A.

D-E. Distributions of doubling times, obtained as in Figure 2D, for populations of MC4100ΔclpB + ClpB-YFP cells that were either not stressed (blue) or kanamycin-stressed (red).

F. The distributions of the differences $\Delta\sigma$, obtained as in A. and used to statistically test the increase in population diversity, σ, under kanamycin stress for MC4100ΔclpB + ClpB-YFP population.

G-H. Heatmaps, obtained as in Figure 2C, for populations of wild-type (MC4100) cells at 37℃ and heat-stressed at 42℃. The colorbar is the same as in **M.**

I-K. Distributions of doubling times, obtained as in Figure 2D, for populations of wild-type cells at 37℃ (blue) and heat-stressed at 42℃(red).

L. The distributions of the differences $\Delta\sigma$, obtained as in A. and used to statistically test the increase in population diversity, σ, under heat stress.

M-P. Figures corresponding to H-L, but in response to kanamycin stress.

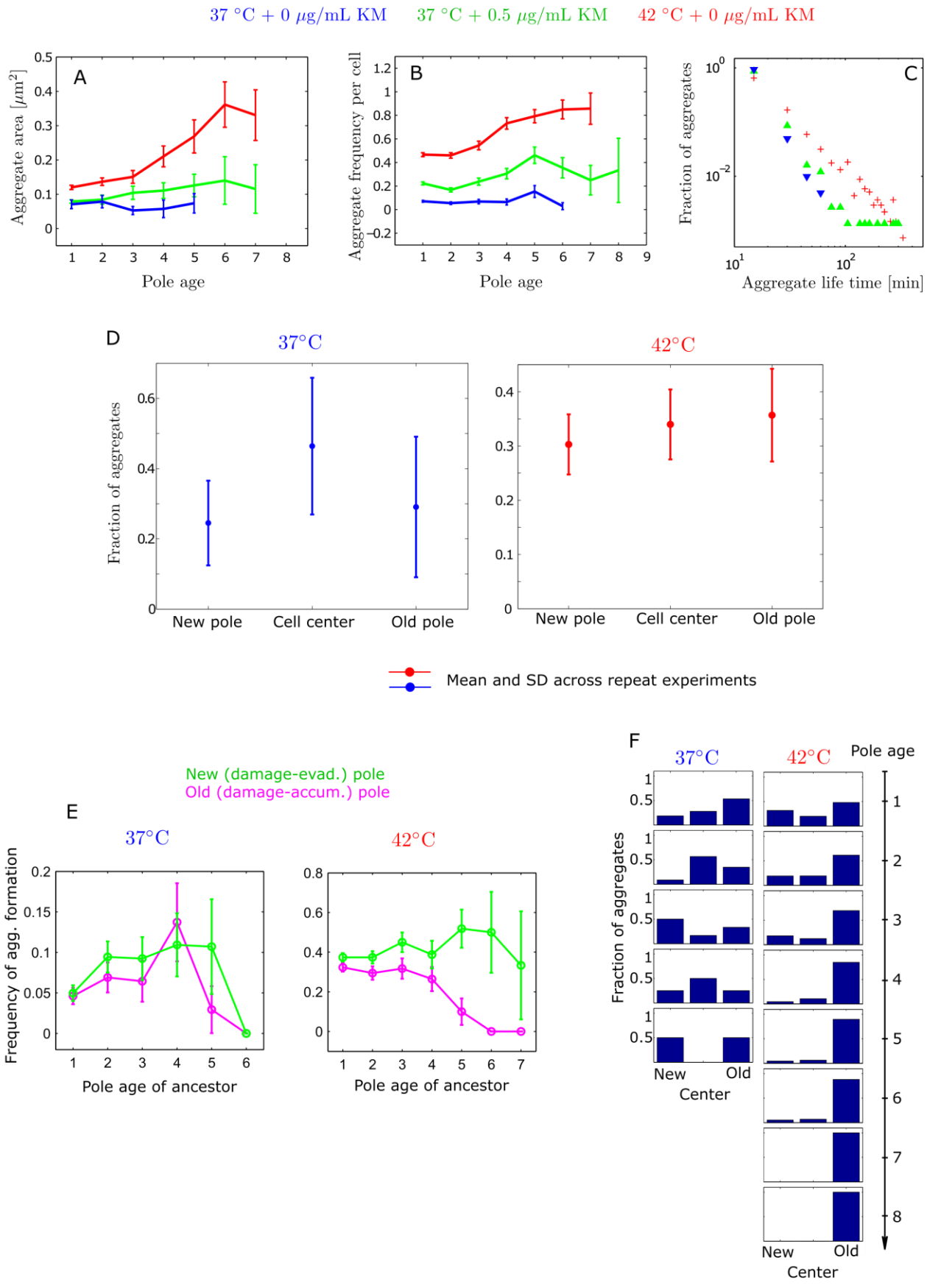
37 °C + 0 μg/mL KM
37 °C + 0.5 μg/mL KM
42 °C + 0 μg/mL KM
A
Aggregate area [μm²]
Pole age
B
Aggregate frequency per cell
Pole age
C
Fraction of aggregates
Aggregate life time [min]
D
37°C
42°C
Fraction of aggregates
New pole
Cell center
Old pole
Mean and SD across repeat experiments
E
New (damage-evad.) pole
Old (damage-accum.) pole
37°C
42°C
Frequency of agg. formation
Pole age of ancestor
F
37°C
42°C
Pole age
Fraction of aggregates
New
Old
Center

Figure S4. Dynamics of Protein Aggregates Provides Mechanistic Explanation of Stress-Induced ADS, Related to Figure 4.

A. Aggregate size increases with pole age and under stress. This confirms the model assumption that damage gradually increases through the old-pole lineage. Errorbars indicate 95% confidence interval.

B. Supporting figure to main Figure 4E, showing the frequency of aggregates in kanamycin-stressed cells. Errorbars indicate standard deviation (see Methods).

C. Supporting figure to main Figure 4C, showing the stability of aggregates in kanamycin-stressed cells.

D. Aggregates are equally likely to form in any of the three regions of the cell. Dots mark the mean over all colonies and errorbars represent standard deviation, quantifying colony-colony variations.

E. Frequency of formation of new aggregates for sister cells as a function of the pole-age of their common ancestor. Frequency at 37℃ and 42℃ is nominally constant, except for old-pole cells at 42℃ where we observe a decrease for older pole ages, corresponding to the increasing frequency of inheritance f^{inh} seen in the main Figure 5B. Errorbars indicate standard deviation (see Methods).

F. Fraction of all aggregates found in the three intracellular regions at each pole age. Aggregates passively move to the old pole after a few divisions when aggregate inheritance is prevalent (42℃) but cannot do this when the aggregates are short-lived and the inheritance is thus insignificant (37℃). This confirms the earlier observations by Lindner *et al.* [2].

All data is sampled in the mutant strain MC4100ΔclpB + ClpB-YFP.

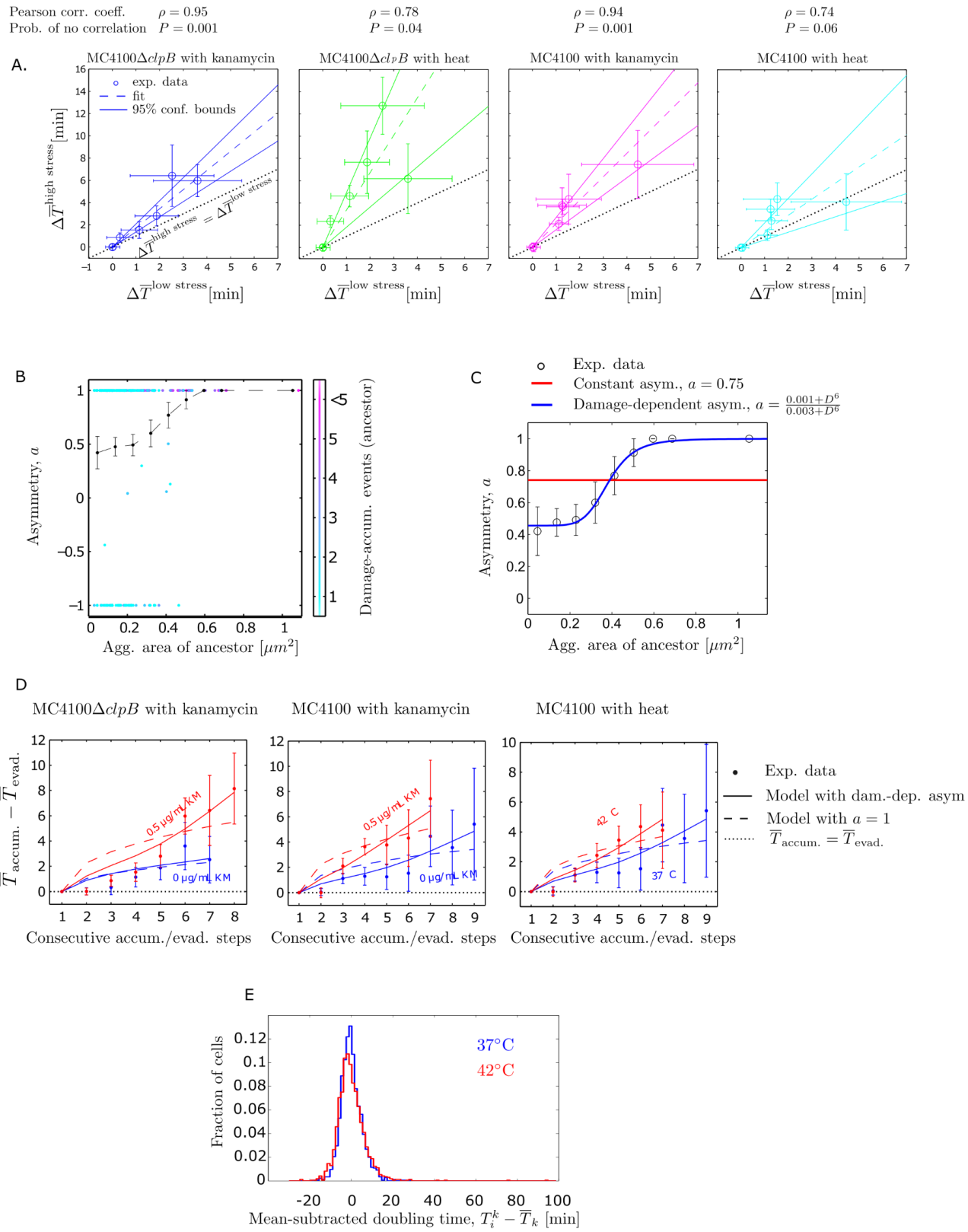

Figure S5. Model Validation Steps, Related to Figure 5.

A. Model and data agree on the near-linear correlation between mean doubling time difference of

consecutive damage accumulating/evading lineages under low and high stress ($\Delta\bar{T}^{high\ stress} \propto \Delta\bar{T}^{low\ stress}$, see Sec. III.6). Circles are the means and errorbars are the standard error of the means. Dashed lines are the error-weighted best fits and full lines are 95% confidence interval.
Pearson linear correlation coefficient ρ and the associated probabilities P of having a similar value of ρ under the null hypothesis of no correlation between the low-stress and high-stress data indicate statistically significant (positive) linear correlation between low-stress and high-stress conditions across all investigated strains and stresses at the 5 % level.
B. Supplementary figure to main Figure 5C. Experimental measurements of average asymmetry $\langle a \rangle = \frac{A_{OP}^{inh} - A_{NP}^{inh}}{A_{OP}^{inh} + A_{NP}^{inh}}$, where A_{OP}^{inh} and A_{NP}^{inh} is the total are of inherited aggregates to the old-pole and new-pole offspring, respectively.
C. Lines show the best fits of the models with constant (red) and damage-dependent (blue) asymmetry.
B.-C. Errorbars mark standard deviation.
D. Supplemental to main Figure 5A. Difference $\Delta\bar{T}$ of doubling times of extreme-branch lineages in the population tree for both low (blue) and high stress (red) obtained from experimental data (filled circles). The parameters inferred from model fits are summarized in Table S2. Dashed lines give result using model with constant asymmetry ($a = 1$) while full lines shows a superior result from model with damage-dependent asymmetry.
E. Quantification of ADS-unrelated noise through the distribution of ``centered" doubling times (for MC4100ΔclpB). For each cell, the mean of the lineage-group is subtracted from the measured doubling time: $\tilde{T}_i^k = T_i^k - \bar{T}^k$, where T_i^k is the doubling time of cell i in lineage group k and $\bar{T}^k$ is the mean doubling time in lineage group k.